Desalination 555 (2023) 116523

Contents lists available at ScienceDirect

Desalination

journal homepage: www.elsevier.com/locate/desal

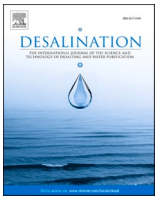

Performance assessment and modeling of an SWRO pilot plant with an energy recovery device under variable operating conditions

A. Ruiz-García [a,*], I. Nuez [a], M. Khayet [b,c]

[a] Department of Electronic Engineering and Automation, University of Las Palmas de Gran Canaria, Campus Universitario de Tafira, E-35017 Las Palmas de Gran Canaria, Spain
[b] Department of Structure of Matter, Thermal Physics and Electronics, Faculty of Physics, University Complutense of Madrid, Avda. Complutense s/n, 28040 Madrid, Spain
[c] Madrid Institute for Advanced Studies of Water (IMDEA Water Institute), Calle Punto Net N° 4, 28805, Alcalá de Henares, Madrid, Spain

HIGHLIGHTS

- Experimental data of a full-scale SWRO desalination plant with ERD
- Performance assessment of SWRO desalination plant with ERD under variable operation
- ANN based model for predicting Qp and Condp was developed.
- SEC varied from 3.21 to 4.47 kWh m^{-3} for a wide range of operation of SWRO plant.

GRAPHICAL ABSTRACT

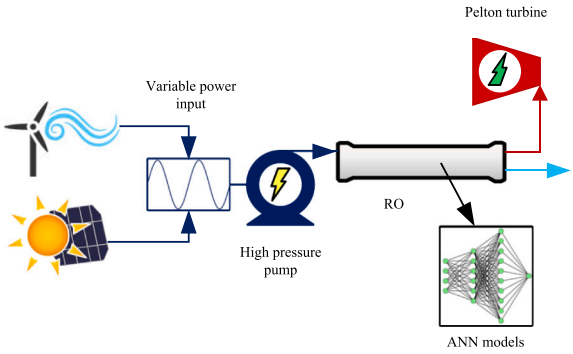

ARTICLE INFO

Keywords:
Desalination
Reverse osmosis
Energy recovery device
Variable operation
Renewable energy
Artificial neural networks

ABSTRACT

Reverse osmosis (RO) is one of the most widespread desalination technologies in use today due to its good performance and reliability. Given that it is an energy intensive technology, using variable renewable energy sources (VRES) to power RO systems is an interesting option. Work with the RO system under variable operating conditions is one of the strategies that can be employed to take advantage of all the energy that is available at any given time from an off-grid renewable system. However, this will entail additional challenges in terms of, among other factors, plant maintenance and permeate production rate and quality. In grid-connected seawater RO (SWRO) desalination plants, energy recovery devices (ERD) are commonly used to increase energy efficiency performance. In these cases, the ERD usually operates under constant operating conditions. This work aims to assess the performance of an SWRO system with an ERD under widely variable operating conditions. The SWRO system has six membrane elements in pressure vessels. The ERD is a Pelton turbine connected to a generator to measure the energy produced by the turbine. An artificial neural network (ANN) based model was developed to estimate the performance of the SWRO-ERD system under variable operating conditions. According to the results, power savings of between 2.9 and 6.08 kW can be achieved for a wide range of operating conditions, allowing an increase in the produced permeate flux (Q_p). The proposed ANN-based model is able to estimate Q_p and permeate

* Corresponding author.
E-mail addresses: alejandro.ruiz@ulpgc.es (A. Ruiz-García), ignacio.nuez@ulpgc.es (I. Nuez), khayetm@fis.ucm.es (M. Khayet).

https://doi.org/10.1016/j.desal.2023.116523
Received 21 November 2022; Received in revised form 17 February 2023; Accepted 25 February 2023
Available online 9 March 2023

electrical conductivity with error intervals of 1.56×10^{-6} - 8.49×10^{-2} $m^3 h^{-1}$ and 8.33×10^{-5} - 31.06 μS cm^{-1}, respectively. The experimental data and the developed model could help to obtain a better performance prediction of VRES-powered SWRO systems that are operating under variable operating conditions and with ERDs.

Nomenclature

Acronyms

ANN	artificial neural network
ERD	energy recovery device
HL	hidden layer
HPP	high pressure pump
PV	pressure vessel
RES	renewable energy sources
RO	reverse osmosis
SWRO	seawater reverse osmosis
VFD	variable frequency drive
A	average water permeability coefficient (m Pa^{-1} s^{-1})
B	average solute permeability coefficient (m s^{-1})
$Cond$	conductivity (μS cm^{-1})
C	concentration (mg L^{-1})
D	solute diffusivity (m^2 s^{-1})
d_h	hydraulic diameter of feed channel (m)
h	feed-brine spacer height (m)
I	electric current (A)
J	flux per unit area (m^3 m^{-2} s^{-1})
k	mass transfer coefficient
MAE	mean absolute error
$MAPE$	mean absolute percentage error (%)
MSE	mean square error
n	number of estimated values
p	pressure (Pa)
P_{in}	power input to high pressure pump (kW)
Q	flow (m^3 h^{-1})
R	flux recovery (%)
Sc	Schmidt number
SDI	silt density index
SEC	specific energy consumption (kW h m^{-3})
Sh	Sherwood number
S_m	membrane surface (m^2)
TCF	temperature correction factor
TDS	total dissolved solids (mg L^{-1})
TMP	transmembrane pressure (Pa)
T	temperature (°C)
$y_{i,est}$	estimated values
$y_{i,exp}$	observed values

Greek letters

Δp	pressure drop (Pa)
η	dynamic viscosity (kg m^{-1} s)
π	osmotic pressure (Pa)
ρ	density (kg m^{-3})
ε	porosity in feed channel
nu	velocity (m s^{-1})

Subscripts

b	brine
f	feed
m	membrane
p	permeate

1. Introduction

Desalination is a key strategy to satisfy water demand in countries with high levels of water stress and periodic water shortages [1]. Worldwide, desalinated water production is still growing significantly. For instance, the desalination projects tendered out in the first six months of 2019 showed a capacity of 4 million m^3 d^{-1}. This quantity is close to the total of 2015 and 2016 combined [1]. Faced with an ever increasing water demand, interest in seawater desalination continues to grow. Among the available industrial seawater desalination technologies, the most frequently used is reverse osmosis (RO) because of its reliability and lower specific energy consumption (*SEC*) [2,3]. Despite being an efficient process in terms of energy consumption compared to other technologies, seawater reverse osmosis (SWRO) remains an energy intensive process that has been associated with the emission of greenhouse gases as well as other environmental impacts [4,5]. The fight against climate change is just one of the compelling reasons for the interest in using renewable energy sources (RES) for the powering of SWRO systems [6,7].

Currently, using RES to power SWRO systems is far from simple, and its feasibility depends on numerous factors that include accessibility to water and energy [1], costs [8,9], regulations [10], etc. The most common RES applied to desalination are wind, solar, geothermal and tidal/wave [11]. Various configurations of RES-SWRO systems have been adopted. Maleki et al. [12] proposed a cost-effective hybrid energy system comprising photovoltaic/wind/hydrogen RES to power RO desalination plants. Padrón et al. [13] studied a hybrid system which was based on photovoltaic modules, different wind turbines supplemented with battery banks and the possible inclusion of diesel generators if required. The HOMER hybrid optimization model tool was used to find the optimal design of this hybrid system. An optimization study to manage a photovoltaic/wind/battery/RO-based hybrid system was carried out by Peng et al. [14]. The SWRO desalination plants powered by RES commonly use the generated electricity, which is intermittent and variable over the course of a day. This fluctuation can be compensated for by connecting SWRO desalination plants to the power grid, allowing their steady-state operation [15]. When this option is not possible, in isolated regions, the SWRO desalination plants powered by RES are in off-grid systems and their operation is essentially intermittent [16]. In some cases, the SWRO-RES systems are equipped with batteries for energy storage [17] to extend their operating time. In intermittent operation there are two ways to operate SWRO desalination plants, under permanent (i.e. constant feed pressure (p_f) and flow rate (Q_f)) [18] or variable operating conditions (variable p_f and Q_f) [19]. The first option allows the desalination plant to operate under given design conditions, but battery use is important as the input power required for the operation is usually high. On the other hand, operating an SWRO desalination plant under variable operating conditions would allow use of lower power inputs, reducing the dependence on batteries. In both cases, batteries could provide smoother operating conditions [20]. Operating an SWRO system under variable/intermittent conditions is complex because of the need to control important factors such as permeate production rate, permeate quality in terms of total dissolved solids (*TDS*) and fouling effects on RO performance [21–23]. This complication is increased if an energy recovery device (ERD) is installed

since the operation of the ERD would also be variable as well as its performance.

Nuez et al. [24] studied the variable operation of an SWRO system which was connected to a wind turbine with no energy storage system or ERD and found that the applied feed pressures of 39, 49 and 60 bar resulted in water flux recovery (R) rates of 19.74, 31.37 and 40 %, respectively, with a permeate electrical conductivity between 429 and 292 μS cm^{-1}, and with the lower values at pressures close to 60 bar. Ntavou et al. [25] undertook a performance analysis of a multi-skid SWRO unit with variable power input using an ERD based on axial piston pumps coupled with axial piston motors. Filmtec™ SW30-4040 membranes and a model saline feed solution of 37,500 mg L^{-1} were used. It was observed that the lower the power input (P_{in}) the higher the specific energy consumption (*SEC*), ranging between around 3.5 and 6 kWh m^{-3} for three different feed temperatures (T_f). Dimitriou et al. [19] carried out a validation study of a theoretical model for the prediction of SWRO system performance under variable operating conditions. The Filmtec™ SW30-4040 membrane was used, as in the previous study, but in this case a small-scale SWRO unit was used with a single pressure vessel (PV) and Clark pump unit as ERD. The applied p_f ranged between 35 and 45 bar and the obtained *TDS* of the permeate varied between 200 and 600 g m^{-3}. However, the corresponding *SEC* data were not provided. The same SWRO system with air pressure vessels as energy storage device was used by Karavas et al. [26]. In this case, the applied p_f ranged between 39 and 51 bar, and the obtained permeate electrical conductivity varied between 200 and 1000 μS cm^{-1}, while the *SEC* varied from 6 to 14 kWh m^{-3}. Calise et al. [27] did an economic evaluation of SWRO desalination using photovoltaic panels as power source. The analysis of the performance of the SWRO system with ERI® (pressure exchanger that transfers pressure energy from brine stream to feed stream) as ERD employed a simulation that used the Dupont® Water Application Value Engine (WAVE) software together with a model that the authors of the study proposed. They assumed a constant value of 2.2 kWh m^{-3} for *SEC*. Considering a product water price of 7 € m^{-3}, the payback period obtained was about 1.3 years. To maximize system performance, the authors recommended reducing the range of operating pressures that start up the RO system which showed similar results. *SEC* was taken as a constant value of 2.2 kWh m^{-3}. Monjezi et al. [28] proposed an off-grid solar energy system to power an SWRO desalination plant with integrated photovoltaic thermal cooling. They carried out simulations of the system with the Reverse Osmosis System Analysis (ROSA) software. For the Filmtec SW30–2540 membrane, an R of 40 % was obtained for single-stage operation with *SEC* reduction from 4.27 to 4.15 kWh m^{-3} when using photovoltaic thermal cooling. Delgado-Torres et al. [29] undertook a preliminary SWRO study using a hybrid (photovoltaic-tidal) system. ROSA was also used for a simulation of the SWRO system performance without ERD, considering two SWRO membranes: Filmtec™ SW30HRLE– 440i and Filmtec SW30XLE – 440i. According to the results obtained with ROSA, *SEC* was 3.5 kWh m^{-3}. Schallenberg-Rodríguez et al. [30] studied the energy supply from RES to an SWRO desalination plant with the ERI® PX pressure exchanger and considering intermittent operating conditions. A *SEC* of 3.84 kWh m^{-3} was considered for sizing the RES facility. There are two main types of ERDs, centrifugal and isobaric. Among the centrifugal options, the Pelton turbine stands out with a yield of between 85 and 90 % at its nominal operating point. Among the isobaric ERDs, the RO Kinetic®, DWEER™, ERI® PX and iSave stand out with yields of up to 98 % at their nominal operating points. It should be noted that the Pelton turbine is a well established and flexible operating device, the RO Kinetic® is not commercially available, the DWEER is designed for high flow rates (> 160 $m^3 h^{-1}$), the iSave is noisy (87 dB), and the performance of the ERI® PX varies considerably under variable operating conditions and so calibration is needed [31]. Most installed ERDs in RO desalination plants work under steady operating conditions, showing a stable performance most of the time. With isobaric ERDs and under steady operating conditions, the achieved *SEC* could be in the range 2.5–4.0 kWh m^{-3} for full-scale SWRO desalination plants [32]. Efforts are still being made to develop improved ERDs [33–35], but there is a lack of information about the performance of this type of device in full-scale RO desalination plants operating under variable operating conditions. In isolated SWRO-RES systems under variable operating conditions, it is important to have an ERD that does not need any adjustments and allows flexible operation without large fluctuations in performance. In general, ERDs are not evaluated under variable operating conditions, which could be an operational mode of an off-grid SWRO system powered by RES.

The modeling of RES-SWRO systems is key to estimate their performance under hypothetical real conditions. The variable operation of RES-SWRO systems makes it complex to model these systems using standard transport phenomena equations as it is common not to have all the devices required to measure every single variable that affects their operation. In addition, it is necessary to obtain a lot of information in real time from the RO systems that helps to estimate the performance. An in-depth understanding of a system is not required with machine learning techniques such as artificial neural network (ANN) based models, which allow the modeling of complex and nonlinear systems [36,37]. The basic idea behind ANN-based models is to use multiple layers of interconnected neurons to approximate a non-linear function that maps inputs to outputs. During the training process, the weights of the connections are updated based on the error between the network's predicted outputs and the ground truth outputs, using an optimization algorithm such as the stochastic gradient descent. A large number of studies have been published involving the use of ANN-based models and RO desalination plants [38]. Murthy and Vora [39], who proposed an ANN-based model for predicting solute rejection and permeate flow (Q_p), used as input parameters p_f, feedwater concentration (C_f) and Q_f. The model had two hidden layers (HL) of 10 neurons each. The log-sigmoid activation function was used and the Lavenberg-Marquardt algorithm for training. Another ANN-based model was developed by Libotean et al. [40], with one HL and three neurons to estimate the performance in terms of salt passage and Q_p of a pilot plant with a two-stage RO system. The operating parameters were T_f, p_f, Q_f and the feedwater electrical conductivity ($Cond_f$). Khayet et al. [41] proposed the use of predictive models based on response surface methodology (RSM) and ANNs for estimating solute rejection and Q_p. The input parameters were the C_f, T_f, p_f and Q_f of an RO pilot plant. The ANN-based model had two HLs with five and three neurons respectively and one output. RSM and ANNs are both used for modeling and prediction in various fields. However, RSM is a simpler, faster and more interpretable method for modeling and prediction, while ANN is a more powerful and flexible method that can handle more complex relationships and larger amounts of data. The choice of method depends on the specific requirements of the problem and the available data. Garg and Joshi [42] also carried out a comparison between RSM and an ANN model. The model that was developed aimed to predict the R, *SEC* and solute rejection considering four inputs, pH, C_f, p_f and T_f. The ANN-based model had one HL with five neurons. Madaeni et al. [43] used the experimental data of a full-scale brackish water reverse osmosis (BWRO) desalination plant to develop an ANN-based model for predicting Q_p and permeate electrical conductivity ($Cond_p$). The model inputs were operating time (t), transmembrane pressure (*TMP*), $Cond_f$ and Q_f. The ANN-based model had two HLs with eleven and five neurons respectively and two outputs. Reasonably high correlation coefficients were found between the experimental and predicted responses for Q_p and $Cond_p$ (0.94 and 0.96, respectively). Data of five small and large BWRO desalination plants were used by Aish et al. [44] to develop an ANN to predict the performance in terms of the solute rejection factor and Q_p. The obtained ANN-based model had one HL with six neurons and one output. For the solute rejection factor, differences of 0.96 and 11.25 mg L^{-1} were detected between the observed and predicted values. Choi et al. [45] modeled a full-scale RO desalination plant considering an ANN model with one HL, ten neurons and one output for predicting relative p_f, relative pressure drop (Δp) and relative C_p (relative parameters were the

ratio between the values and reference value). The precision of the proposed model was quantified by means of the standard deviation of error and R^2, with the two parameters in a range between 0.014 and 0.065 and between 0.92 and 0.95, respectively. ANN-based models have also been developed for predicting the contaminants of wastewater treated by an RO process [46,47].

The aim of this paper is to evaluate the performance of a full-scale SWRO system with a Pelton turbine as ERD operating under variable operating conditions, and to develop an ANN model based on some of the obtained experimental data.

2. Material and methods

2.1. Plant description

The SWRO desalination plant is situated in the southeast of Gran Canaria (Canary Islands, Spain). A bypass of an existing full-scale SWRO desalination plant was made to feed the pilot plant used in this study. The pilot SWRO desalination plant (Fig. 1) had one stage and one PV with six SWRO membrane modules (Koch Fluid Systems TFC 2822-SS). The high pressure pump (HPP CAT 6761) had a three-phase 30 kW electric motor and a variable frequency drive (VFD model ATV-58HD46N4, Telemecanique now Schneider Electric). This plant was tested in a previous work without an ERD and with a regulation valve in the brine line [48] (OPRODES project). The membrane modules were replaced and a Pelton turbine (Fig. 2) was installed in the brine line leaving the regulation valve inoperative. This ERD was not connected directly to the HPP (shaft connection), but was coupled to the 30 kW electric motor that worked as a generator to measure the turbine-generated power. This power was measured for a flow range between 0.96 and 24 $m^3\ h^{-1}$ and a pressure range of 5.07–7.09 MPa. The Pelton turbine was not connected to the HPP because the ERD was installed later (the SWRO system was working without an ERD for a while), and so connection between the turbine and HPP was not possible. The variable operating conditions were reached by means of the variable frequency drive of the HPP. Currents between 28 and 57.4 A were set in the VFD. This forced the electric motor connected to the HPP to rotate between 1000 and 1500 rpm. The pressure transmitters and indicators (PI) were installed in both the feed and brine lines, while the temperature transmitter and indicator (TI, type RTD Pt-100) was installed in the feed line. The flow transmitters and indicators (FI, from Endress and Hauser type Promag 30, model 99) were installed in both the permeate and brine lines, while the conductivity transmitters and indicators (CI, from Rosemount Analytical) were installed in the three lines, feed, brine and permeate (Fig. 3). The programmable logic controller used for data acquisition was the TSX Micro 3722 model from Telemecanique.

Fig. 1. SWRO desalination pilot plant.

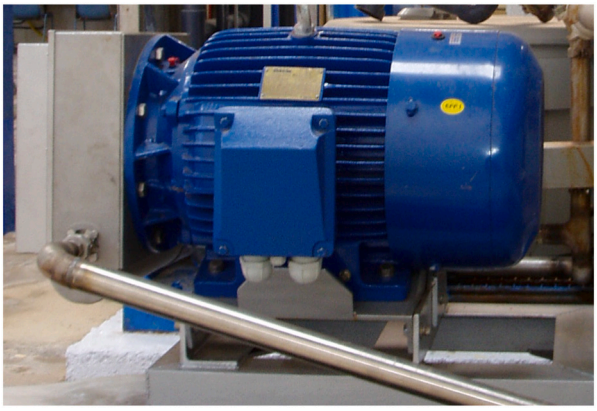

Fig. 2. Pelton turbine coupled with the generator.

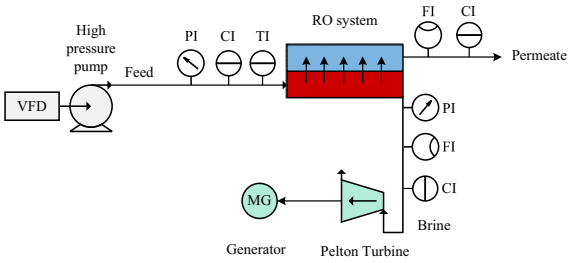

Fig. 3. Flow diagram of the SWRO pilot plant.

2.2. Experimental data and calculations

First, the ERD was tested under a wide range of operating conditions, namely brine pressure (p_b) and brine flow (Q_b), to obtain the generated power. This was done to check the performance decay for the entire operating range of the ERD. Experimental data such as the T_f, p_f, p_b, Q_p, Q_b, $Cond_p$, $Cond_f$, brine electrical conductivity ($Cond_b$), and electric current consumed by the VFD (I) were collected each 30 s. Fig. 3 shows the instrumentation in the RO system. A feedwater sample analysis published in a previous work using the same SWRO desalination plant was considered (Table 1). The experimental runs were carried out keeping the R around 42 % and increasing the rotation speed of the electric motor from 1000 rpm to 1500 rpm.

To evaluate the performance of the SWRO pilot plant, the average water permeability coefficient (A) and the average solute permeability coefficient (B as NaCl) were calculated using the following equations [49,50].

$$m = 1.0069 - 2.757 \cdot 10^{-4} \cdot T_f \quad (1)$$

$$\rho = 498.4 \cdot m + \sqrt{248400 \cdot m^2 + 752.4 \cdot m \cdot C_{fb}} \quad (2)$$

where m is the molal concentration (mol kg^{-1}), ρ is the average feed-

Table 1
Feed water inorganic composition.

Ion	Concentration (mg L^{-1})
Ca^{2+}	429.67
$Mg^{2}+$	1342.85
Na^{+}	9900
K^{+}	320
HCO_3^-	169.6
$SO_4^{=}$	2653.45
Cl^-	17,377.17
SiO_2	44.5
TDS	32,237.34

brine density (kg m^{-2}) and C_{fb} is the feed-brine concentration (average between C_f and permeate concentration (C_p)). $Cond_f$ and $Cond_b$ (μS cm^{-1}) were measured. To estimate the respective C (mg L^{-1}) on the basis of the conductivity values, a factor of 0.7 was used in accordance with [51]). C_p was calculated by multiplying $Cond_p$ by 0.51.

$$\eta = 1.234{\cdot}10^{-6}{\cdot}exp\left(0.00212{\cdot}C_{fb} + \frac{1965}{273.15+T_f}\right) \quad (3)$$

$$D = 6.725{\cdot}10^{-6}{\cdot}exp\left(0.1546{\cdot}10^{-3}{\cdot}C_{fb} - \frac{2513}{273.15+T_f}\right) \quad (4)$$

$$Sc = \frac{\eta}{\rho{\cdot}D} \quad (5)$$

$$d_h = \frac{4\varepsilon}{\frac{2}{h} + (1-\varepsilon)\frac{8}{h}} \quad (6)$$

where η is the dynamic viscosity (kg m^{-1} s^{-1}), D is the solute diffusivity (m^2 s^{-1}), Sc is the Schmidt number, d_h the feed channel hydraulic diameter (m), ε the porosity of the cross section area in the feed channel (0.89 [52]) and h the feed channel height, which was taken as 28 milli-inches (7.11 × 10^{-4} m) for the SWRO membrane module TFC 2822-SS. Koutsou et al. [53] proposed some correlations to estimate Sh for different feed spacer geometries. Information about feed spacer geometries of this membrane was not found, and so one of the correlations proposed in [53] was used (Eq. (8)). Eqs. (2), (3) and (4) were taken from [54].

$$Re = \frac{\rho{\cdot}\nu{\cdot}d_h}{\eta} \quad (7)$$

$$Sh = \frac{k{\cdot}d_h}{D} = 0.14{\cdot}Re^{0.64}{\cdot}Sc^{0.42} \quad (8)$$

$$\frac{C_m - C_p}{C_f - C_p} = exp(J_w/k) \quad (9)$$

The temperature correction factor (TCF) was calculated as follows [55]:

If $T \geqslant 25°C$:

$$TCF = exp\left[2,640{\cdot}\left(\frac{1}{298} - \frac{1}{273+T}\right)\right] \quad (10)$$

If $T \leqslant 25°C$:

$$TCF = exp\left[3,020{\cdot}\left(\frac{1}{298} - \frac{1}{273+T}\right)\right] \quad (11)$$

$$B = \frac{C_p{\cdot}Q_p}{(C_m - C_p){\cdot}S_m{\cdot}TCF} \quad (12)$$

$$A = \frac{J_w}{\left(p_f - \frac{\Delta p_{fb}}{2} - p_p - \pi_m + \pi_p\right){\cdot}TCF} \quad (13)$$

where Re is the Reynolds number, k is the mass transfer coefficient of solute, C_m is the concentration at the membrane surface (mg L^{-1}), J_w is the permeate flux (m^3 m^{-2} s^{-1}), S_m is the membrane area (m^2), Δp_{fb} is the average feed-brine pressure drop in the feed channel (Pa), p_p is the permeate pressure (this was not measured but was taken as 35 kPa), π_m is the average osmotic pressure (Pa) at the membrane surface, and π_{ps} is the permeate osmotic pressure (Pa). All osmotic pressures were calculated considering the concentration as NaCl according to the detailed information reported by the American Society for Testing and Materials (ASTM) [56]. Both the permeability coefficients, A and B, were calculated at 25 °C (applying the adopted TFC) so that the results could be comparable with other experimental studies carried out under different operating temperatures.

2.3. ANN-based model of the SWRO pilot plant

The proposed ANN-based model has 4 inputs (4 neurons), $Cond_f$, p_f, Q_f and T_f (Fig. 4). The model was used to estimate Q_p and $Cond_p$ (outputs) separately, with two ANNs (one for each output). The architecture of the selected ANN is a multilayer perceptron with a feedforward structure [57]. Two hidden layers of neurons were selected given that, in theory, there is no justification to use more, as one hidden layer is the most appropriate for most problems [58,59]. It should be noted that most RO-ANN studies have considered one or two hidden layers [60–62]. More specific criteria to choose the number of hidden layers would require further testing [63]. The tan-sigmoid activation function (or transfer function) was used for the neurons in the hidden layer, while the purelin function was used for the output layer. The performance function (Eq. (14)) to evaluate the proposed ANN model was the mean square error (*MSE*) (Eq. (15)). The mean absolute error (*MAE*) (Eq. (16)) and the mean absolute percentage error (*MAPE*) were also calculated.

!

$$MSE = \frac{1}{n}\sum_{i=1}^{n}\left(y_{i,exp} - y_{i,est}\right)^2 \quad (14)$$

$$MAE = \frac{\sum_{i=1}^{n}\left|\left(y_{i,exp} - y_{i,est}\right)\right|}{n} \quad (15)$$

$$MAPE = \frac{100}{n}\sum_{i=1}^{n}\left|\frac{y_{i,exp} - y_{i,est}}{y_{i,est}}\right| \quad (16)$$

where n is the number of estimated values, $y_{i,\,exp}$ is the observed value, and $y_{i,\,est}$ is the estimated value. A genetic algorithm was considered to set the minimum number of neurons in each hidden layer that minimize the *MSE*. The aforementioned algorithm was implemented in Matlab's Global Optimization Toolbox through the ga function [64]. The initial population (default 0.05 times the population size) was generated randomly with a uniform distribution. Two HLs of neurons were selected after checking that better results were obtained with 2 as opposed to 1. The number of neurons in both HLs ranged between 1 and 100. The training block comprised 70 % of the experimental runs with 15 % set aside each for validation and testing. It was decided to use the Levenberg-Marquardt backpropagation training algorithm after checking that it gave the best results.

3. Results and discussion

3.1. Experimental results and performance analysis

Fig. 5 shows the generated power of the Pelton turbine for different p_b and Q_b values. Membrane manufacturers typically set a maximum Q_f

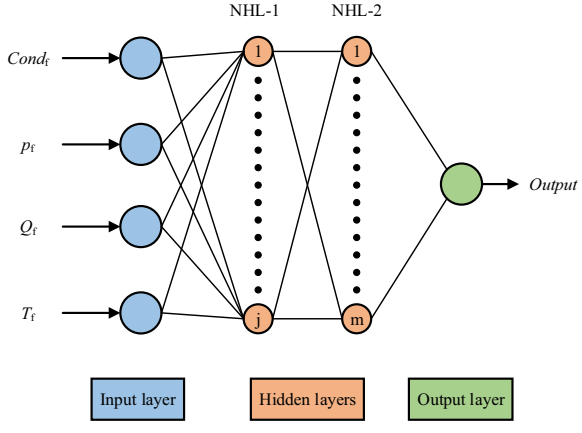

Fig. 4. Schematic representation of the ANN-based model.

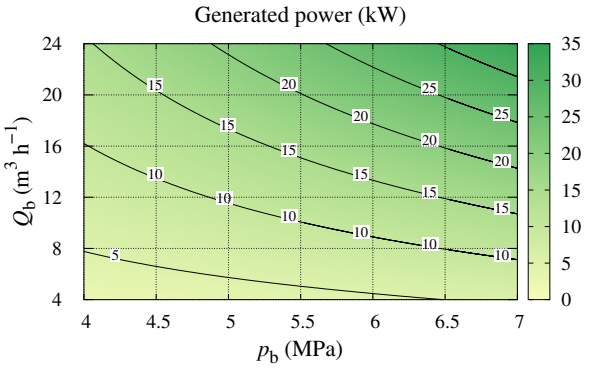

Fig. 5. Power generated by the Pelton turbine for its entire operating range.

that depends on the silt density index (*SDI*) of the feed dilution. Maximum feed flows are around 12 m^3 h^{-1} per PV for a feed solution with *SDI*≤3 [65]. Taking into consideration this data, the ERD could operate with an SWRO system of 1 PV to 4 PVs. For a p_b range of 4–7 MPa, the performance decay of the ERD was about 16 %.

During the operating time, T_f was between 16 and 17 °C. The $Cond_f$ was between 40,656 and 45,650 µS cm^{-1} (i.e. C_f range of 28.46–31.95 g L^{-1} considering a conversion factor of 0.7). These variations affected the performance of the SWRO plant due to the osmotic pressure variation along the operating time. Fig. 6 shows Q_p for different p_f operating values ranging from 4.8 to 6.5 MPa and Q_f in the range 5.8–9.4 m^3 h^{-1}. The obtained Q_p varied from 2.3 to 4.1 m^3 h^{-1}. It should be mentioned that different Q_p for the same P_{in} to the HPP were obtained due to variation of T_f and pH_f, since at higher T_f Q_p increases for the same p_f due to its effect on the coefficient *A* and the variations of pH_f may cause the rejection of some solutes to vary as the form in which the ion is found varies, as is the case with boron [50], These variations could also be caused to a lesser extent by the uncertainty of the measuring devices as is usual in this type of SWRO desalination plant. In addition, the operating conditions through the pre-treatment step resulted in some changes to the flow and pressure conditions at the inlet of the HPP. This affected HPP power consumption (P_{in}), as can be seen in Fig. 7 which shows the effects of Q_f and p_f on P_{in}. For the aforementioned range of P_{in} (11.2–22.96 kW), the HPP induced a Q_f in the range of 5.8–9.4 m^3 h^{-1} with a p_f between 4.8 and 6.5 MPa. The relation between the power input to the SWRO system (input to PV) and P_{in} was between 68.3 and 79.5 %. It should be noted that pressure values in the input of the HPP were not measured. These values would allow to obtain more precise calculations about the performance of the HPP. It was considered that the pressure at the input of the HPP was 0, and so all power was supposedly supplied by the HPP. In general, Q_p increased with higher P_{in}. The reverse situation was observed for $Cond_p$, as plotted in Fig. 8. The obtained $Cond_p$ was in the range 259–432 µS cm^{-1}. Considering a

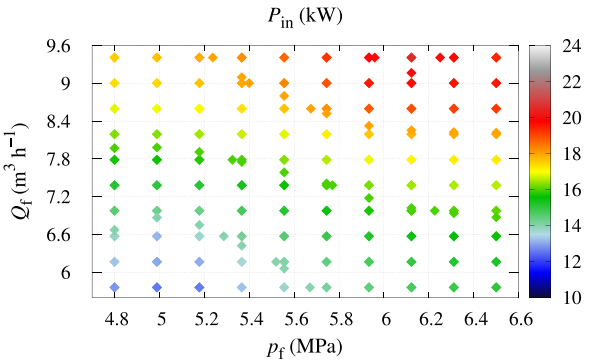

Fig. 7. Effects of Q_f and p_f on the power consumed by HPP.

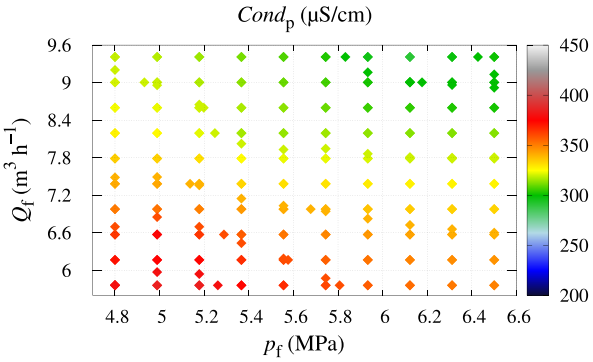

Fig. 8. $Cond_p$ for different p_f and Q_f operating values.

conversion factor of 0.51 to estimate C_p, the corresponding range was 131.2–220.3 mg L^{-1}. Fig. 9 shows the power generated by the ERD for different Q_b and p_b operating conditions. This generated power varied between 2.09 and 6.08 kW for different Q_b and p_b values in the range of 4.7–6.4 MPa and 3.2–5.5 m^3 h^{-1}, respectively. It should be considered that the connection between the ERD and the HPP was not taken into account and an additional loss in power management should be included. Fig. 10 shows the *SEC* of the SWRO pilot plant with and without the ERD, with respective results in the range 3.21–4.47 and 4.41–6.03 kWh m^{-3}, respectively. When an SWRO system is powered by RES, typically the goal is to maximize Q_p while maintaining an appropriate permeate quality for a given P_{in}. By operating the SWRO pilot plant with ERD, a more than 25 % enhancement of Q_p was achieved. Obtaining a proper permeate quality may be challenging under variable operating conditions, and such a challenge increases when less rejected ions such as boron [50] and fluorine [66–68] are considered.

Fig. 11 shows the relation between the coefficients *A* and *B* at 25 °C.

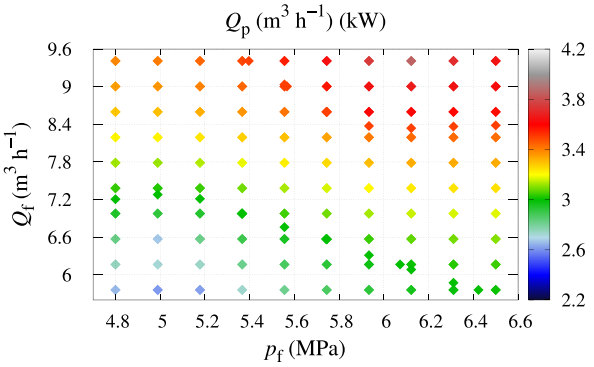

Fig. 6. Q_p for different Q_f and p_f operating values.

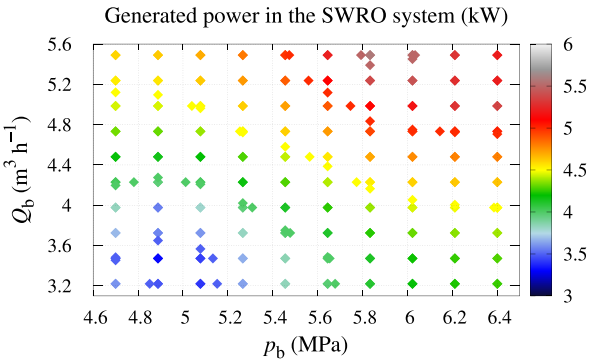

Fig. 9. Power generated by the ERD vs Q_b and p_b.

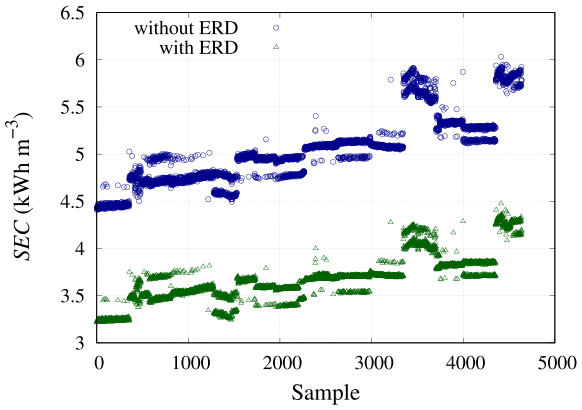

Fig. 10. *SEC* of the SWRO pilot plant with and without ERD.

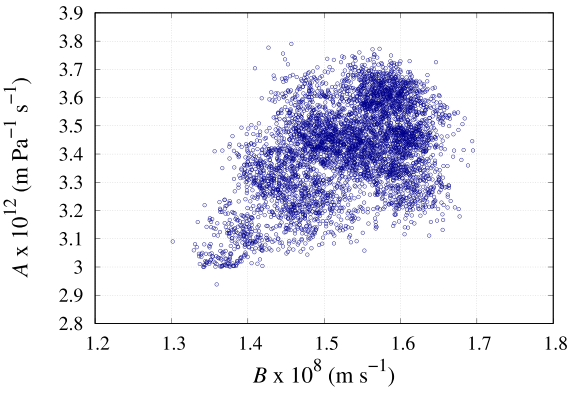

Fig. 11. *A* vs *B*.

Under the applied variable operating conditions, no clear trend could be plotted between *A* and *B*. This may be attributable to the variable operating conditions of the SWRO pilot plant in terms of *TMP*, C_f and flow patterns. This unusual behavior also occurs when SWRO systems are powered under variable P_{in}, for instance, when using renewable energy sources such as wind and solar [25,69–71]. In this case, coefficient *A* was in the range between 2.94×10^{-12} and 3.79×10^{-12} m Pa^{-1} s^{-1} and *B* between 1.30×10^{-8} and 1.69×10^{-8} m s^{-1}. Without considering the *TCF*, the ranges were between 2.32×10^{-12} and 2.90×10^{-12} m Pa^{-1} s^{-1} and between 1.02×10^{-8} and 1.31×10^{-8} m s^{-1} for *A* and *B*, respectively. These values are not competitive compared with SWRO membranes currently available in the market.

3.2. ANN-based model

Table 2 shows the architecture and errors of the ANN-based model for the two outputs Q_p and $Cond_p$. The results obtained for Q_p were better than those for $Cond_p$. This is due to the precision and noise associated to the electrical conductivity meters, which is normal when measuring relatively high electrical conductivities as opposed to flow meters whose recording signal is less noisy. Another important factor that affects $Cond_p$ is the pH of the feed aqueous solution. Probably, the measurement and inclusion of this parameter in the model would have helped to obtain a better $Cond_p$ estimation. However, taking into consideration a conversion factor of 0.51 between $Cond_p$ and C_p, the error interval was in a range of 4.2461×10^{-5} - 15.8409 mg L^{-1}, which is a reasonably acceptable approximation. In order to be more specific in terms of quality criteria in the permeate, ion determination in real time would be needed to create predictive models. However, it is not common to measure ions in real time in full-scale RO desalination plants as it increases the costs. It should be considered that the weights obtained for the model are only valid for this plant and under the described operating conditions. If greater temperature changes occur in the feed water and/or the membranes become dirty, causing changes in their permeability coefficients, the model must be refitted to obtain new weights. Figs. 12 and 13 show the experimental and predicted values of Q_p and $Cond_p$ for 4637 samples by the developed ANN-based model. A stable estimation of Q_p can be observed along the whole operating range, whereas for $Cond_p$ higher deviations can be detected, especially for samples close to 1000 and 2900. A weak point is that during the experimental work T_f remained fairly constant, and so the model may not identify how considerable changes in T_f affect the parameters Q_p and $Cond_p$. To take this into account, a longer operating time would be necessary, although *TCF* could give an estimation. In full-scale RO desalination plants, feedwater conditions can change from one day to another which, together with the imprecision of electrical conductivity measurements, makes it complex to develop a more accurate estimator for $Cond_p$. However, the advantage is that the experiments were carried out in actual operating conditions of full-scale desalination plants and not in controlled environments such as those in laboratories. Generally, models developed for laboratory pilot plants can present difficulties in estimating the real behavior of large-scale plants.

Table 2
Structure of the ANN-based model and errors.

	NHL-1	*NHL-2*	*MSE*	*MAE*	*MAPE* (%)	Error range
Q_p (m^3 h^{-1})	49	94	1.3070×10^{-4}	0.0082	3.7780×10^{-4}	1.5618×10^{-6} - 0.0849
$Cond_p$ (μS cm^{-1})	40	59	45.5962	5.0335	8.6847×10^{-4}	8.3258×10^{-5} - 31.0605

4. Conclusions

In this study, an analysis was conducted of the performance of SWRO desalination pilot plant with an ERD and operating under variable operating conditions, providing useful information about such systems. The variability of the results obtained shows how challenging it is to predict the behavior of an SWRO system working under a wide operating range. These data should be taken into consideration when SWRO desalination plants are powered by variable RES. It should be considered that the operating period was short in comparison with full-scale SWRO desalination plants, which may be in operation with the same SWRO membranes for more than five years. Also, taking into consideration the operating conditions in the inlet of the HPP by controlling the pretreatment stage would help to have a better approach in predicting the behavior of the desalination plant. Performance losses due to fouling

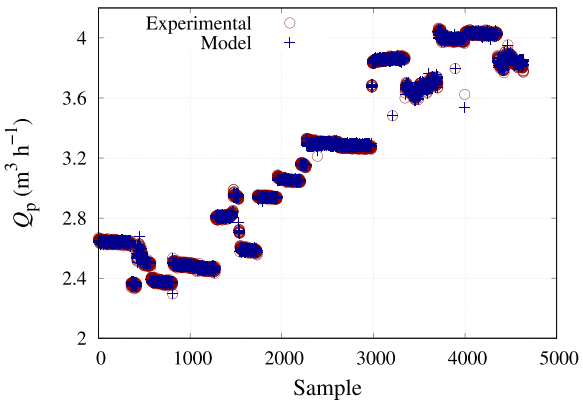

Fig. 12. Experimental and estimated values by the ANN-based model for Q_p.

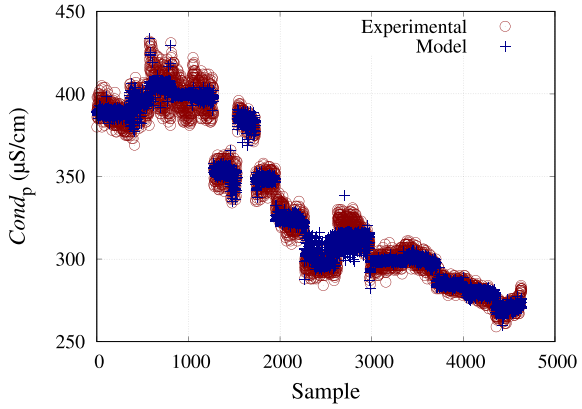

Fig. 13. Experimental and estimated values by the ANN-based model for $Cond_p$.

should additionally be considered when designing this kind of SWRO-RES plant. The proposed ERD, comprising a Pelton turbine coupled to a generator, is an acceptable device for SWRO desalination plants working under wide operating ranges due to its stable performance and low maintenance. An ANN-based model is proposed for the estimation of Q_p and $Cond_p$. Model validation was performed with the experimental data, making it reliable for the estimation of the aforementioned parameters in full-scale SWRO desalination plants. Unfortunately, the experimental runs were not long enough to take into consideration the effect of fouling on full-scale SWRO membranes under variable operating conditions. Further research, considering fouling, would be needed to develop long-term predictive models for SWRO-RES under variable operation and using ERDs. This would help to improve the viability of this type of system and provide a more realistic performance estimation of SWRO-RES plants.

Declaration of competing interest

The authors declare that they have no known competing financial interests or personal relationships that could have appeared to influence the work reported in this paper.

Data availability

Data will be made available on request.

Acknowledgements

This research was co-funded by the ERDF and the ACLIEMAC Project (MAC2/3.5b/380) of the INTERREG V-A MAC 2014-2020 program.

References

[1] H. Nassrullah, S.F. Anis, R. Hashaikeh, N. Hilal, Energy for desalination: a state-of-the-art review, Desalination 491 (2020), 114569, https://doi.org/10.1016/j.desal.2020.114569.
[2] E.J. Okampo, N. Nwulu, Optimisation of renewable energy powered reverse osmosis desalination systems: a state-of-the-art review, Renew. Sust. Energ. Rev. 140 (2021), 110712, https://doi.org/10.1016/j.rser.2021.110712.
[3] A. Ruiz-García, I. Nuez, Simulation-based assessment of safe operating windows and optimization in full-scale seawater reverse osmosis systems, Desalination 533 (2022), 115768, https://doi.org/10.1016/j.desal.2022.115768.
[4] G. Amy, N. Ghaffour, Z. Li, L. Francis, R.V. Linares, T. Missimer, S. Lattemann, Membrane-based seawater desalination: present and future prospects, Desalination 401 (2017) 16–21, https://doi.org/10.1016/j.desal.2016.10.002, 50th anniversary of Desalination.
[5] N. Najid, S. Fellaou, S. Kouzbour, B. Gourich, A. Ruiz-García, Energy and environmental issues of seawater reverse osmosis desalination considering boron rejection: a comprehensive review and a case study of exergy analysis, Process Saf. Environ. Prot. 156 (2021) 373–390, https://doi.org/10.1016/j.psep.2021.10.014.
[6] J. Bundschuh, M. Kaczmarczyk, N. Ghaffour, B. Tomaszewska, State-of-the-art of renewable energy sources used in water desalination: present and future prospects, Desalination 508 (2021), 115035, https://doi.org/10.1016/j.desal.2021.115035.
[7] M.T. Mito, X. Ma, H. Albuflasa, P.A. Davies, Variable operation of a renewable energy-driven reverse osmosis system using model predictive control and variable recovery: towards large-scale implementation, Desalination 532 (2022), 115715, https://doi.org/10.1016/j.desal.2022.115715.
[8] K. Elmaadawy, K.M. Kotb, M. Elkadeem, S.W. Sharshir, A. Dán, A. Moawad, B. Liu, Optimal sizing and techno-enviro-economic feasibility assessment of large-scale reverse osmosis desalination powered with hybrid renewable energy sources, Energy Convers. Manag. 224 (2020), 113377, https://doi.org/10.1016/j.enconman.2020.113377.
[9] H. Rezk, M. Alghassab, H.A. Ziedan, An optimal sizing of stand-alone hybrid PV-fuel cell-battery to desalinate seawater at saudi NEOM City, Processes 8 (4) (2020) 1–19, https://doi.org/10.3390/pr8040382.
[10] S. Sen, S. Ganguly, Opportunities, barriers and issues with renewable energy development - a discussion, Renew. Sust. Energ. Rev. 69 (2017) 1170–1181, https://doi.org/10.1016/j.rser.2016.09.137.
[11] A. Ali, R.A. Tufa, F. Macedonio, E. Curcio, E. Drioli, Membrane technology in renewable-energy-driven desalination, Renew. Sust. Energ. Rev. 81 (2018) 1–21, https://doi.org/10.1016/j.rser.2017.07.047.
[12] A. Maleki, F. Pourfayaz, M.H. Ahmadi, Design of a cost-effective wind/photovoltaic/hydrogen energy system for supplying a desalination unit by a heuristic approach, Sol. Energy 139 (2016) 666–675, https://doi.org/10.1016/j.solener.2016.09.028.
[13] I. Padrón, D. Avila, G.N. Marichal, J.A. Rodríguez, Assessment of hybrid renewable energy systems to supplied energy to autonomous desalination systems in two islands of the canary archipelago, Renew. Sust. Energ. Rev. 101 (2019) 221–230, https://doi.org/10.1016/j.rser.2018.11.009.
[14] W. Peng, A. Maleki, M.A. Rosen, P. Azarikhah, Optimization of a hybrid system for solar-wind-based water desalination by reverse osmosis: comparison of approaches, Desalination 442 (2018) 16–31, https://doi.org/10.1016/j.desal.2018.03.021.
[15] A.M. Abdelshafy, H. Hassan, J. Jurasz, Optimal design of a grid-connected desalination plant powered by renewable energy resources using a hybrid PSO–GWO approach, Energy Convers. Manag. 173 (2018) 331–347, https://doi.org/10.1016/j.enconman.2018.07.083.
[16] W. Lai, Q. Ma, H. Lu, S. Weng, J. Fan, H. Fang, Effects of wind intermittence and fluctuation on reverse osmosis desalination process and solution strategies, Desalination 395 (2016) 17–27, https://doi.org/10.1016/j.desal.2016.05.019.
[17] A. Mostafaeipour, M. Qolipour, M. Rezaei, E. Babaee-Tirkolaee, Investigation of off-grid photovoltaic systems for a reverse osmosis desalination system: a case study, Desalination 454 (2019) 91–103, https://doi.org/10.1016/j.desal.2018.03.007.
[18] B. Peñate, F. Castellano, A. Bello, L. García-Rodríguez, Assessment of a stand-alone gradual capacity reverse osmosis desalination plant to adapt to wind power availability: a case study, Energy 36 (7) (2011) 4372–4384, https://doi.org/10.1016/j.energy.2011.04.005.
[19] E. Dimitriou, P. Boutikos, E.S. Mohamed, S. Koziel, G. Papadakis, Theoretical performance prediction of a reverse osmosis desalination membrane element under variable operating conditions, Desalination 419 (2017) 70–78, https://doi.org/10.1016/j.desal.2017.06.001.
[20] N. Ghaffour, S. Lattemann, T. Missimer, K.C. Ng, S. Sinha, G. Amy, Renewable energy-driven innovative energy-efficient desalination technologies, Appl. Energy 136 (2014) 1155–1165, https://doi.org/10.1016/j.apenergy.2014.03.033.
[21] M. Freire-Gormaly, A. Bilton, Design of photovoltaic powered reverse osmosis desalination systems considering membrane fouling caused by intermittent operation, Renew. Energy 135 (2019) 108–121, https://doi.org/10.1016/j.renene.2018.11.065.
[22] B.S. Richards, D.P. Capão, W.G. Früh, A.I. Schäfer, Renewable energy powered membrane technology: impact of solar irradiance fluctuations on performance of a brackish water reverse osmosis system, Sep. Purif. Technol. 156 (2015) 379–390, https://doi.org/10.1016/j.seppur.2015.10.025.
[23] J. Shen, A. Jeihanipour, B.S. Richards, A.I. Schäfer, Renewable energy powered membrane technology: experimental investigation of system performance with variable module size and fluctuating energy, Sep. Purif. Technol. 221 (2019) 64–73, https://doi.org/10.1016/j.seppur.2019.03.004.
[24] I. de la Nuez Pestana, F.Javier García Latorre, C.Argudo Espinoza, A.Gómez Gotor, Optimization of RO desalination systems powered by renewable energies. Part i: Wind energy, Desalination 160 (3) (2004) 293–299, https://doi.org/10.1016/S0011-9164(04)90031-8.
[25] E. Ntavou, G. Kosmadakis, D. Manolakos, G. Papadakis, D. Papantonis, Experimental evaluation of a multi-skid reverse osmosis unit operating at fluctuating power input, Desalination 398 (2016) 77–86, https://doi.org/10.1016/j.desal.2016.07.014.
[26] C.-S. Karavas, K.G. Arvanitis, G. Kyriakarakos, D.D. Piromalis, G. Papadakis, A novel autonomous PV powered desalination system based on a DC microgrid concept incorporating short-term energy storage, Sol. Energy 159 (2018) 947–961, https://doi.org/10.1016/j.solener.2017.11.057.
[27] F. Calise, F.L. Cappiello, R. Vanoli, M. Vicidomini, Economic assessment of renewable energy systems integrating photovoltaic panels, seawater desalination and water storage, Appl. Energy 253 (2019), 113575, https://doi.org/10.1016/j.apenergy.2019.113575.
[28] A.A. Monjezi, Y. Chen, R. Vepa, A.E.-H.B. Kashyout, G. Hassan, H.E.-B. Fath, A.E.-W. Kassem, M.H. Shaheed, Development of an off-grid solar energy powered reverse osmosis desalination system for continuous production of freshwater with

integrated photovoltaic thermal (PVT) cooling, Desalination 495 (2020), 114679, https://doi.org/10.1016/j.desal.2020.114679.
[29] A.M. Delgado-Torres, L. García-Rodríguez, M.J. del Moral, Preliminary assessment of innovative seawater reverse osmosis (SWRO) desalination powered by a hybrid solar photovoltaic (PV) - tidal range energy system, Desalination 477 (2020), 114247, https://doi.org/10.1016/j.desal.2019.114247.
[30] J. Schallenberg-Rodríguez, B. Del Rio-Gamero, N. Melian-Martel, T. Lis Alecio, J. González Herrera, Energy supply of a large size desalination plant using wave energy. Practical case: north of gran canaria, Appl. Energy 278 (2020), 115681, https://doi.org/10.1016/j.apenergy.2020.115681.
[31] S. Arenas Urrea, F. Díaz Reyes, B. Peñate Suárez, J.A. de la Fuente Bencomo, Technical review, evaluation and efficiency of energy recovery devices installed in the canary islands desalination plants, Desalination 450 (2019) 54–63, https://doi.org/10.1016/j.desal.2018.07.013.
[32] R.S. Adha, T.-T. Nguyen, C. Lee, I.S. Kim, High recovery and fouling resistant double stage seawater reverse osmosis: an inter-stage erd configuration optimized with internally-stage design (isd), Desalination 521 (2022), 115401, https://doi.org/10.1016/j.desal.2021.115401.
[33] D. Song, Y. Zhang, H. Wang, L. Jiang, C. Wang, S. Wang, Z. Jiang, H. Li, Demonstration of a piston type integrated high pressure pump-energy recovery device for reverse osmosis desalination system, Desalination 507 (2021), 115033, https://doi.org/10.1016/j.desal.2021.115033.
[34] Z. Sun, Y. Wang, J. Zhou, Z. Xu, S. Xu, Development and operational stability evaluation of new three-cylinder energy recovery device for SWRO desalination system, Desalination 502 (2021), 114909, https://doi.org/10.1016/j.desal.2020.114909.
[35] N. Liu, Z. Liu, Y. Li, L. Sang, Development and experimental studies on a fully-rotary valve energy recovery device for SWRO desalination system, Desalination 397 (2016) 67–74, https://doi.org/10.1016/j.desal.2016.06.026.
[36] J. Jawad, A.H. Hawari, S. Javaid Zaidi, Artificial neural network modeling of wastewater treatment and desalination using membrane processes: a review, Chem. Eng. J. 419 (2021), 129540, https://doi.org/10.1016/j.cej.2021.129540.
[37] S. Al Aani, T. Bonny, S.W. Hasan, N. Hilal, Can machine language and artificial intelligence revolutionize process automation for water treatment and desalination? Desalination 458 (2019) 84–96, https://doi.org/10.1016/j.desal.2019.02.005.
[38] C. Niu, X. Li, R. Dai, Z. Wang, Artificial intelligence-incorporated membrane fouling prediction for membrane-based processes in the past 20 years: a critical review, Water Res. 216 (2022), 118299, https://doi.org/10.1016/j.watres.2022.118299.
[39] Z. Murthy M. M. Vora , Prediction of reverse osmosis performance using artificial neural network, Indian J. Chem. Technol.
[40] D. Libotean, J. Giralt, F. Giralt, R. Rallo, T. Wolfe, Y. Cohen, Neural network approach for modeling the performance of reverse osmosis membrane desalting, J. Membr. Sci. 326 (2) (2009) 408–419, https://doi.org/10.1016/j.memsci.2008.10.028.
[41] M. Khayet, C. Cojocaru, M. Essalhi, Artificial neural network modeling and response surface methodology of desalination by reverse osmosis, J. Membr. Sci. 368 (1) (2011) 202–214, https://doi.org/10.1016/j.memsci.2010.11.030.
[42] M.C. Garg, H. Joshi, A new approach for optimization of small-scale RO membrane using artificial groundwater, Environ. Technol. 35 (23) (2014) 2988–2999, pMID: 25189847. arXiv:doi:.
[43] S.S. Madaeni, M. Shiri, A.R. Kurdian, Modeling, optimization, and control of reverse osmosis water treatment in kazeroon power plant using neural network, Chem. Eng. Commun. 202 (1) (2015) 6–14, https://doi.org/10.1080/00986445.2013.828606, arXiv.
[44] A.M. Aish, H.A. Zaqoot, S.M. Abdeljawad, Artificial neural network approach for predicting reverse osmosis desalination plants performance in the Gaza strip, Desalination 367 (2015) 240–247, https://doi.org/10.1016/j.desal.2015.04.008.
[45] Y. Choi, Y. Lee, K. Shin, Y. Park, S. Lee, Analysis of long-term performance of full-scale reverse osmosis desalination plant using artificial neural network and tree model, Environ. Eng. Res. 25 (5) (2020) 763–770.
[46] A.T. Mohammad, M.A. Al-Obaidi, E.M. Hameed, B.N. Basheer, I.M. Mujtaba, Modelling the chlorophenol removal from wastewater via reverse osmosis process using a multilayer artificial neural network with genetic algorithm, J. Water Process. Eng. 33 (2020), 100993, https://doi.org/10.1016/j.jwpe.2019.100993.
[47] V. Sivanantham, P. Narayana, K.J. Hyeong, P. Pareddy, V. Sangeetha, M. Kyoung – Seok, K.H. In, H.K. Sung, N. Reddy, Modeling and optimization of chlorophenol rejection for spiral wound reverse osmosis membrane modules, Chemosphere 268 (2021), 129345, https://doi.org/10.1016/j.chemosphere.2020.129345.
[48] F.J.García Latorre, S.O.Pérez Báez, A.Gómez Gotor, Energy performance of a reverse osmosis desalination plant operating with variable pressure and flow, Desalination 366 (2015) 146–153, https://doi.org/10.1016/j.desal.2015.02.039, energy and Desalination.
[49] Y. Du, L. Xie, J. Liu, Y. Wang, Y. Xu, S. Wang, Multi-objective optimization of reverse osmosis networks by lexicographic optimization and augmented epsilon constraint method, Desalination 333 (1) (2014) 66–81, https://doi.org/10.1016/j.desal.2013.10.028.
[50] A. Ruiz-García, I. Nuez, Performance evaluation and boron rejection in a SWRO system under variable operating conditions, Comput. Chem. Eng. 153 (2021), 107441, https://doi.org/10.1016/j.compchemeng.2021.107441.
[51] A.F. Rusydi, Correlation between conductivity and total dissolved solid in various type of water: a review, in: IOP Conference Series: Earth and Environmental Science, Vol. 118, IOP Publishing, 2018, p. 012019.
[52] G. Schock, A. Miquel, Mass transfer and pressure loss in spiral wound modules, Desalination 64 (1987) 339–352, https://doi.org/10.1016/0011-9164(87)90107-X.
[53] C.P. Koutsou, S.G. Yiantsios, A.J. Karabelas, A numerical and experimental study of mass transfer in spacer-filled channels: effects of spacer geometrical characteristics and schmidt number, J. Membr. Sci. 326 (1) (2009) 234–251, https://doi.org/10.1016/j.memsci.2008.10.007.
[54] M. Taniguchi, M. Kurihara, S. Kimura, Behavior of a reverse osmosis plant adopting a brine conversion two-stage process and its computer simulation, J. Membr. Sci. 183 (2) (2001) 249–257, https://doi.org/10.1016/S0376-7388(00)00597-4.
[55] A.R. Marsh, P.K. Eriksson, Projecting RO desalination system performance with Filmtec spiral-wound elements, in: Proc. of the Seminar on Membrane Processes, 1988.
[56] ASTM, The Annual Book of ASTM Standard, Designation: D 4516-00, 2010.
[57] A. Jain, J. Mao, K. Mohiuddin, Artificial neural networks: a tutorial, Computer 29 (3) (1996) 31–44, https://doi.org/10.1109/2.485891.
[58] T. Masters, Practical Neural Network Recipes in C++, Morgan Kaufmann, 1993.
[59] K. Hornik, M. Stinchcombe, H. White, Multilayer feedforward networks are universal approximators, Neural Netw. 2 (5) (1989) 359–366, https://doi.org/10.1016/0893-6080(89)90020-8.
[60] A. Abbas, N. Al-Bastaki, Modeling of an ro water desalination unit using neural networks, Chem. Eng. J. 114 (1) (2005) 139–143, https://doi.org/10.1016/j.cej.2005.07.016.
[61] Y.G. Lee, Y.S. Lee, J.J. Jeon, S. Lee, D.R. Yang, I.S. Kim, J.H. Kim, Artificial neural network model for optimizing operation of a seawater reverse osmosis desalination plant, Desalination 247 (1) (2009) 180–189, https://doi.org/10.1016/j.desal.2008.12.023.
[62] M. Barello, D. Manca, R. Patel, I. Mujtaba, Neural network based correlation for estimating water permeability constant in ro desalination process under fouling, Desalination 345 (2014) 101–111, https://doi.org/10.1016/j.desal.2014.04.016.
[63] J.C. Principe, N.R. Euliano, W.C. Lefebvre, Neural and Adaptive Systems: Fundamentals Through Simulations Vol. 672, Wiley, New York, 2000.
[64] K. Deep, K.P. Singh, M. Kansal, C. Mohan, A real coded genetic algorithm for solving integer and mixed integer optimization problems, Appl. Math. Comput. 212 (2) (2009) 505–518, https://doi.org/10.1016/j.amc.2009.02.044.
[65] D. W. Solutions , Filmtec Reverse Osmosis Membranes Technical Manual, Dupont Water Solutions: Edina, MN, USA.
[66] Y.-A. Boussouga, B.S. Richards, A.I. Schäfer, Renewable energy powered membrane technology: system resilience under solar irradiance fluctuations during the treatment of fluoride-rich natural waters by different nanofiltration/reverse osmosis membranes, J. Membr. Sci. 617 (2021), 118452, https://doi.org/10.1016/j.memsci.2020.118452.
[67] J. Shen, G. Mkongo, G. Abbt-Braun, S.L. Ceppi, B.S. Richards, A.I. Schäfer, Renewable energy powered membrane technology: fluoride removal in a rural community in northern Tanzania, Sep. Purif. Technol. 149 (2015) 349–361, https://doi.org/10.1016/j.seppur.2015.05.027.
[68] J. Shen, B.S. Richards, A.I. Schäfer, Renewable energy powered membrane technology: case study of st. Dorcas borehole in Tanzania demonstrating fluoride removal via nanofiltration/reverse osmosis, Sep. Purif. Technol. 170 (2016) 445–452, https://doi.org/10.1016/j.seppur.2016.06.042.
[69] F.E. Ahmed, R. Hashaikeh, N. Hilal, Solar powered desalination – technology, energy and future outlook, Desalination 453 (2019) 54–76, https://doi.org/10.1016/j.desal.2018.12.002.
[70] A. Ali, R.A. Tufa, F. Macedonio, E. Curcio, E. Drioli, Membrane technology in renewable-energy-driven desalination, Renew. Sust. Energ. Rev. 81 (2018) 1–21, https://doi.org/10.1016/j.rser.2017.07.047.
[71] J. Leijon, D. Salar, J. Engström, M. Leijon, C. Boström, Variable renewable energy sources for powering reverse osmosis desalination, with a case study of wave powered desalination for Kilifi, Kenya, Desalination 494 (2020), 114669, https://doi.org/10.1016/j.desal.2020.114669.